# We are IntechOpen, the world's leading publisher of Open Access books Built by scientists, for scientists

4,900
Open access books available

124,000
International authors and editors

140M
Downloads

154
Countries delivered to

Our authors are among the
TOP 1%
most cited scientists

12.2%
Contributors from top 500 universities

CLARIVATE ANALYTICS
BOOK CITATION INDEX
INDEXED

WEB OF SCIENCE™

Selection of our books indexed in the Book Citation Index in Web of Science™ Core Collection (BKCI)

Interested in publishing with us?
Contact book.department@intechopen.com

Numbers displayed above are based on latest data collected.
For more information visit www.intechopen.com

# 8

# Image Processing Methods in CT for Radiotherapy Applications

Boussion Nicolas[1,2], Fayad Hadi[2], Le Pogam Adrien[2], Pradier Oliver[1,2] and Visvikis Dimitris[1,2]
[1]*CHU de Brest, Hôpital Morvan, Service de radiothérapie*
[2]*INSERM U650 LaTIM, Brest*
*France*

## 1. Introduction

X-ray computed tomography images (CT) are widely used in radiotherapy planning because they provide electronic densities of tissues of interest which are mandatory to a correct dose computation. Furthermore, the good spatial resolution and soft/hard tissues contrast allow precise target delineation. In this context of dose calculation and delivery, two challenging problems regarding CT images and radiotherapy are adressed here.

First, we present a new automated approach to respiratory motion prediction. Respiratory motion leads to artifacts in the lower part of the lungs and blurs contours of tissues especially in thoracic and upper abdominal cases. Four-dimensional acquisitions allow accounting for this difficulty but at the expense of dosimetric considerations. On the other hand, the knowledge of the organs' motion during radiotherapy treatment is necessary (a) to a good conformation of the isodoses to the target contours and (b) to a sufficient protection of the organs at risk. In this study, we present a model-based method able to predict the internal movement of organs from CT images and external respiratory signals. A promising objective could be the improvement of dose computation and of real-time target tracking during treatment delivery.

In the second part of this work, we present state-of-the-art image combination algorithms able to provide superior information when determining target contours from CT images. The aim is to extract pertinent information from both worlds of medical imaging, morphology and function, and to present them in a single image.

## 2. Respiratory monitoring using predictive models based on 4D CT

### 2.1 Four-dimensional image-based motion management

In external radiotherapy, respiratory-induced organ and tumor motion limits the accuracy of the treatment delivery. This is because, under breathing, the photon beam may from one hand hit on normal tissues while on the other it may miss some of the tumor volume. A solution to this problem is the gating approach (Veda *et al* 2001; Keall *et al* 2002) : the beam is delivered only at a given phase of the breathing cycle, according to an external respiratory signal (pressure belt around the thorax, optical system, active breath-holding). Although this could potentially reduce tumor motion, most patients (especially with lung cancer) have usually

trouble in holding or controlling their breathing. Furthermore the method is rather time consuming. Actually, there is a very interesting alternative to gating which consists of a continuous irradiation of the target during its movement. It is generally referred to as "tumour tracking" and the principle relies on a real-time adjustment of the beam according to a respiratory signal. A number of articles are currently published about this domain of research, but one of the challenging points is the ability to adapt the beam in real-time. Electronic devices, computer methods, and mechanical movements of the LINAC are not sufficiently rapid to allow actual real-time delivery. In this context, we have developped a model which is able to continuously predict the movement of the thorax and the abdomen from a four-dimensional CT exam (4D CT). This approach could help compensating the dead-time problems described previously, just by incorporating reliable tumour position estimates.

The use of 4D CT images reduces the problems caused by respiratory motion and can improve the quality of the radiation therapy (Rietzel et al, 2005). However, 4D CT images correspond to given positions in the respiratory cycle and are not continuous in time. In addition, respiratory cycle irregularities limit the efficiency of 4D CT. To resolve this issue, McClelland et al (McClelland et al, 2006, 2008) worked on the generation of a patient specific model of the motion of the target tumor and the adjacent anatomy. This model provides displacements over the respiratory cycle for any point in the CT volume and is continuous over the respiratory cycle. However this model describes an average respiratory cycle and as such the predictability of the model is limited to the information given by that average respiratory cycle and not the acquired, potentially irregular, respiratory signal. In the study presented in this chapter, we propose an approach based on the creation of a continuous patient specific model that takes into account respiratory signal irregularities while describing, in the same time, respiration induced organ motion. The acquired CT data in cine mode were examined to form continuous CT volumes using a combined phase and amplitude binning procedure based on the information given by a registered respiratory signal (Real-time Position Management: RPM). A B-spline elastic registration is used to spatially register the obtained CT volumes. Finally, the patient specific motion model is reconstructed by performing a 2D fitting for the displacement of every registration control point separately, i.e. every displacement is fitted against the amplitude and the phase values extracted from the acquired respiratory signal. The assumption behind the use of the external respiratory measurements is that a correlation between the acquired respiratory signal and the internal motion exists (Kanoulas et al 2007, Gierga et al 2005). As a result, the issues associated with the non continuous volumes caused by 4D CT acquisitions, and the respiratory signal irregularities, are resolved. This model can hence create a CT volume corresponding to any position in the respiratory cycle using a given respiratory phase and corresponding amplitude.

### 2.2 Description of the methodology

#### 2.2.1 Dataset

The clinical data were acquired on a multislice CT (MSCT) and on a combined PET/CT scanner with a cine CT scan capability. A cine CT scan consists of the continuous acquisition of projections over many gantry rotation cycles while the imaging table remains stationary. As a consequence the X rays do not stop between two continuous axial scans. Each CT scan covers 2cm (8×2.5mm) on an 8-slice MSCT. The duration of each cine CT is normally 1s longer than the average breath cycle, and 19 to 23 images are acquired per slice location. A 0.5s gantry rotation is used for high temporal resolution. The interval between each cine image is 0.45s, and the total reconstruction angle is 360°. Fourteen different slice locations were acquired for

every patient. During the whole acquisition, the time, as well as the amplitude and phase of the patient breathing were recorded. The Realtime Position Management (RPM) system records in addition to the patient respiratory trace, a flag indicating when the CT X-ray tube was on, allowing therefore the time-sampling of the CT data with respect to the respiration phase. A software was developed to examine these acquired 8-slice volumes in order to form 19 (or 23 depending on patient acquisition time) 8 ×14 volumes (512×512×112 voxels, with dimensions 0.97×0.97×2.5 $mm^3$). The obtained CT volume corresponding to the full expiration will be referred to from here onwards as the "reference volume". Moreover, this software removes 8-slice volumes that correspond to irregular breathing (Pan et al, 2007) and then, based on the phase extracted from the respiratory signal and a spline amplitude based interpolation, all CT volumes are reconstructed. The present study includes the analysis of three patients, who were asked to breathe normally and regularly.

### 2.2.2 Elastic registration method

Elastic registration of reconstructed CT volumes is performed using a spatio-temporal algorithm for motion reconstruction from a series of images. This method uses a semi-local spatio-temporal parametric model for the deformation using B-splines and reformulates the registration task as a global optimization problem (Ledesma-Carbayo et al, 2006). The obtained transformation Dt(x) between the frame f(x,t) at time t and the reference frame f(x,0) was defined as a linear combination of B-spline basis functions, located in a rectangular grid (Seungyong et al, 1997):

$$D_t(x) = x + \sum_{j \in Z^N} c_j \beta_r(x / h - j) \tag{1}$$

where $\beta_r(x)$ is a tensor product of centered B-splines of degree r, and j are the indices of the grid locations. Many different transformation grid spacings were tested and finally cubic B-splines with grid spacing set to 5×5×5 pixels provided the best results and were used to represent the deformation.

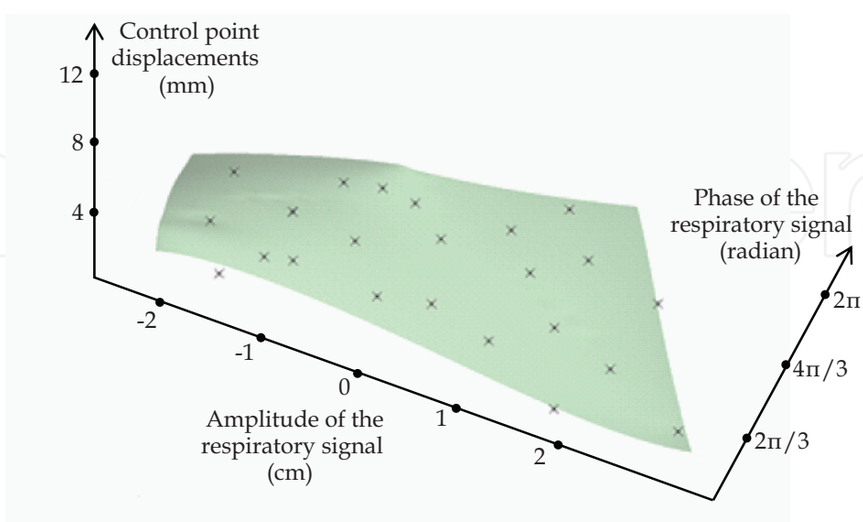


Fig. 1. A 2D-Bspline fitting for one displacement in one direction. The displacement are fitted in function of the phase and amplitude extracted from the respiratory signal.

### 2.2.3 Patient specific motion model

The patient specific motion model is reconstructed by performing a 2D fitting for the x, y and z displacement for every registration control point separately. The value of every displacement is effectively plotted against the amplitude and the phase of the corresponding CT volume and a 2D-Bspline is then fitted to the data. Figure 1 shows an example of this process in the case of a unique displacement in one direction.

Let $\Omega = \{(x,y), 0 \le x < m, 0 \le y < n\}$ be a rectangular domain in the xy-plane. The approximation 2D-Bspline function f is defined by a control lattice Φ in the domain $\Omega$. Let $\phi_{i,j}$ be the value of the ij-th control point on the control lattice Φ located at (i,j) for $i = \{-1, 0, ..., (m+1)\}$ and $j = \{-1, 0, ..., (n+1)\}$. Finally f is defined in terms of these control points by:

$$f(x,y) = \sum_{k=0}^{3}\sum_{l=0}^{3} \beta_k(s)\beta_l(t)\phi_{(i+k)(j+l)} \tag{2}$$

where $i = |x| - 1$, $j = |y| - 1$, $s = x - |x|$, $t = y - |y|$ and βk, βl are uniform cubic b-spline basis function defined as :

$$\beta_0(t) = \frac{1-t^3}{6} \tag{3}$$

$$\beta_1(t) = \frac{3t^3 - 6t^2 + 4}{6} \tag{4}$$

$$\beta_2(t) = \frac{-3t^3 + 3t^2 + 3t + 1}{6} \tag{5}$$

$$\beta_3(t) = \frac{t^3}{6} \tag{6}$$

The patient specific model thus consists of a series of control points that correspond to every displacement in every direction. As a consequence, one can predict the corresponding CT image based on the phase and amplitude of a given respiratory signal. This is simply done by calculating the pixels displacement in all directions based on the different B-spline coefficients and applying them to the reference CT image. The model leads to a non rigid transformation that will alter the reference volume and estimate the CT volume for any position according to an acquired respiratory signal.

### 2.2.4 Evaluation of the methodology

To evaluate the motion model, we have derived CT images using this model having the same amplitude and phase as the acquired CT volumes. These predicted volumes are compared to their corresponding acquired volumes. At each comparison, one of the acquired CT volumes was not included in the motion model creation and was used as a ground truth for comparison purpose only. The correlation coefficient is used for that purpose. It measures a linear affine relation between the intensity of the compared images. The correlation coefficient between two images A and B is given by:

$$\rho(A,B) = \sum_i \sum_j \frac{(i - m_A)(j - m_B)}{\sqrt{\sigma_A}\sqrt{\sigma_B}} pij$$

where $i$ and $j$ are the voxel intensities of images A and B respectively, $m_A$ is the mean of the image intensities, $\sigma_A$ is the standard deviation and $pij$ is the joint probability. A correlation of 1 indicates a perfect matching of the two compared images. In addition to the correlation coefficients, pixel-to-pixel image differences were used to provide global CT image comparisons. Finally, local profiles served to perform local image comparisons between the CT volumes.

### 2.3 First results

In this study results for three patients are presented and for each patient three CT volumes corresponding to different amplitudes and phases were derived using the model. At each prediction step, four different CT volumes were compared; namely the acquired CT (original data: not used in the model creation step), the predicted CT volume using our model, the predicted CT volume using the model based on the use of the phase parameter (phase based model, McClelland et al, 2006) and that derived using the model based on the amplitude parameter (amplitude based model).

Figure 2 shows the coronal view of an original CT image (fig. 2(a)), and the corresponding slices from the derived CT volumes using the new developed model, as well as the phase only and amplitude only based models. The profile results show little advantage from the 2D model in comparison to the 1D amplitude based model, while a more important difference is seen with respect to the 1D phase based model. Figure 3 shows the difference image between the original acquired CT and the predicted image using the 2D model as well as the 1D phase and amplitude based models. Finally, figure 4 shows the analysis on the correlation coefficient results for all three patients between the original and the corresponding model derived CT volumes. The results of both figures 3 and 4 demonstrate a closer matching and better correlation between the original CT volume and the one derived using the 2D model, rather than the 1D phase or amplitude models.

### 2.4 Future work

It is very important to monitor the respiratory movements when delivering radiotherapy treatments in the thorax or in the upper abdomen. Gating and tracking are techniques that lead to a better conformation of the dose to the target, while preserving organs at risk in the same time. In this context, 4D CT images with concomitant recording of the respiratory movements are very useful tools. For this reason we have proposed a patient specific continuous respiratory motion model from such 4D CT acquisitions. The first results show that including both phase and amplitude for the model construction is better than including only one of the two parameters. The demonstration of the efficacy of a 2D model over previous 1D models relies especially on the management of respiratory signal irregularities and on a signal continuity guaranteed during the whole respiratory cycle. The developed model is accurate in describing organ and tumor motion. It is useful for improving the quality of the dose delivery, and it could be of interest also for improving the accuracy of dose calculation. Potential limitations are cases where the correlation between the external acquired respiratory signal and the internal motion is not guaranteed. Numerous studies are currently performed to find the best way to estimate the organ movements from external signals (skin surface etc...). This knowledge will contribute to improve the tumour tracking approaches which are based on personalized predictive models as the one we presented here.

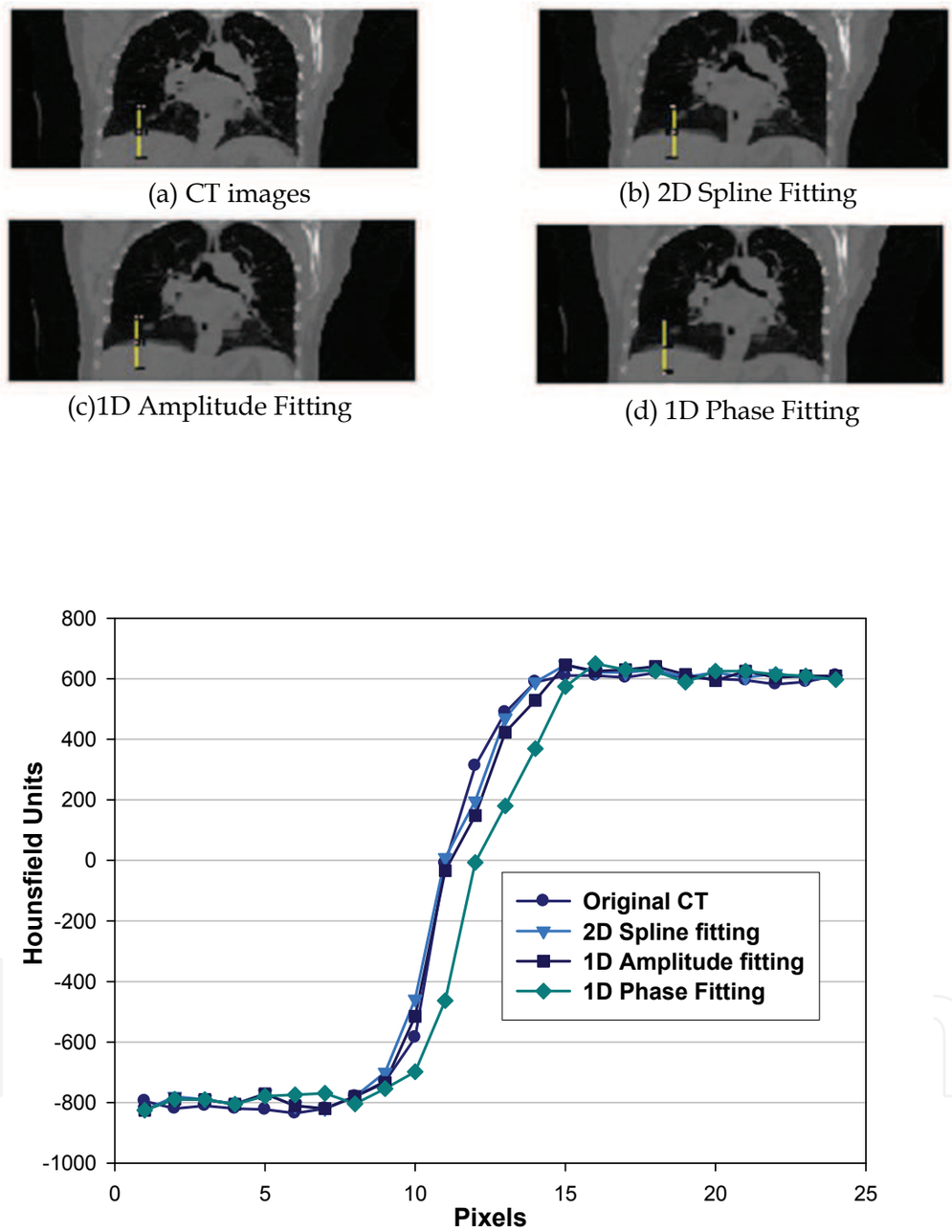


Fig. 2. Coronal view of (a) an original CT image, the same slice from the CT derived from (b) using our 2D model, (c) the phase based model, and (d) using the amplitude based model. In the bottom of the figure we can see the corresponding HU profiles drawn in (a), (b), (c) and (d).

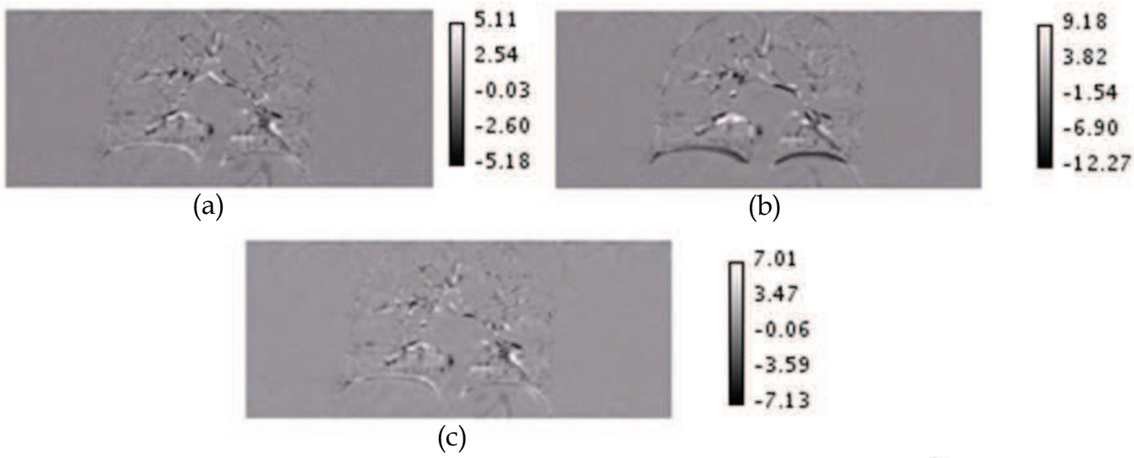


Fig. 3. Coronal view of the difference image between the original CT and the corresponding derived image using (a) our 2D model, (b) the 1D phase only model, and (c) the 1D amplitude only model. Gray pixels indicate areas where images are very similar, while black and white pixels show areas where images differ significantly.

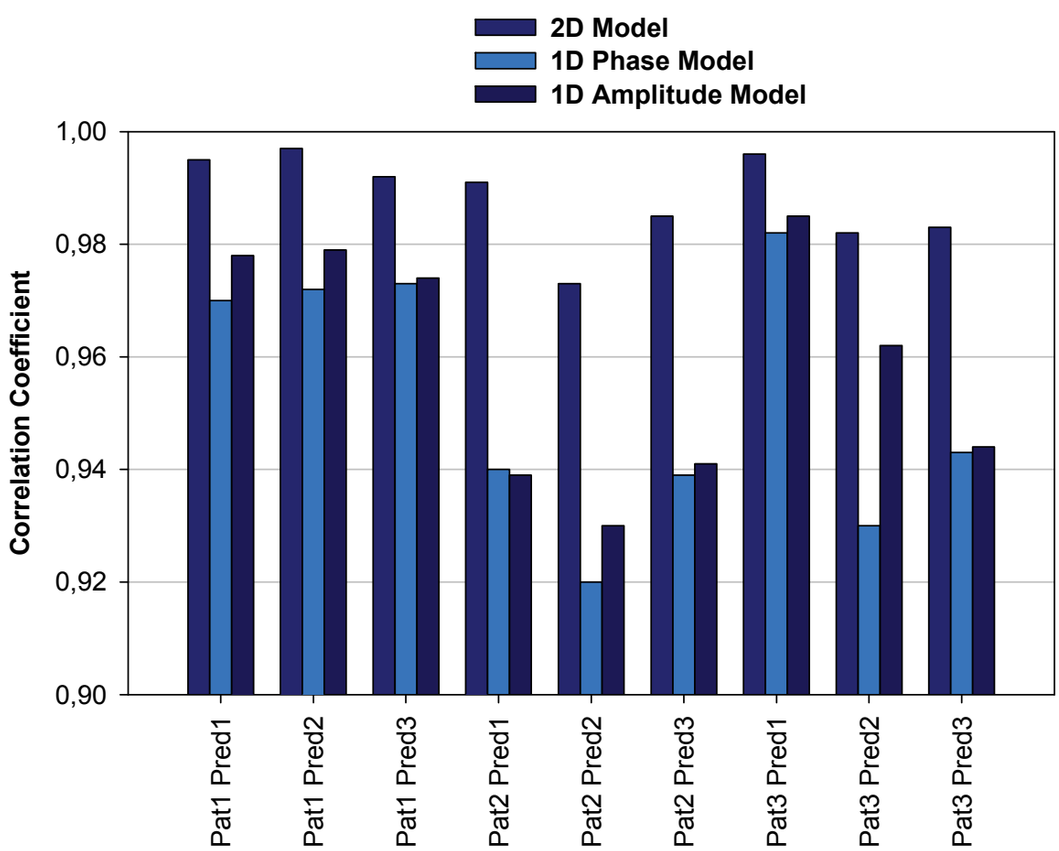


Fig. 4. Comparison of the correlation coefficients derived using the 2D model as well as the 1D phase and amplitude models, for all three patients and for different predicted volume amplitudes and phases.

## 3. Combination of CT with functional images for better delineation of targets in radiotherapy

In radiotherapy, the accurate delineation of the tumours and the organs at risk (OAR) remains a critical step of the treatment planning phase. In a first step, the physician manually or semi-automatically draws regions of interest in the CT images of the patient (target, OAR). Then, the treatment planning system (TPS) is used to compute the dose received by the target and the OAR, the aim being to give the maximum dose to the target while preserving OAR in the same time. During this process, the images obtained by computed tomography are mandatory because they give access to the electronic densities of the tissues, which allows dose calculation by the TPS. CT images also provide valuable anatomical data with good spatial resolution and hard/soft tissues contrast. However, it has been shown that discrepancies often appear between morphological size and shape of the tumor seen in CT, and its functional activity seen in positron emission tomography (PET). The glucose metabolism is for instance obtained in whole-body PET after injection of $^{18}$FDG. In this case, necrotic parts of a tumor may be visible on $^{18}$FDG PET images but not in the CT images. This point is of importance since a higher dose should be delivered to the active part of a tumour than to the necrotic parts. This dose delivery scheme is sometimes referred to as dose painting, i.e. the ability to deliver different levels of dose to different parts of a single target. This dose escalation process leads to a better efficacy especially in prostate cancer for example.

The main difficulty in dose painting is the definition of the target and the delineation of its inner active parts. As already stated, computed tomography gives precise but uniform images while PET is able to segment active/necrotic sub-parts of a given tumour, but with a significantly lower spatial resolution. Images appear more blurred and contours of the different organs are difficult to delineate. These effects are included in what is often referred to as partial volume effects. These latter have several aspects but are mainly caused by the wide point spread function of PET imaging devices from which we define spatial resolution. The full width at half maximum of the point spread function eventually gives the spatial resolution, which may be seen as the ability to separate two points on the reconstructed image. More precisely the spatial resolution is the minimal distance between two actual points inside the patient necessary to separate them on the reconstructed image. If the points are closer than that distance, it is practically impossible to separate them on the image and they appear as a big single blurred point. The aim of the method presented now is to build an enhanced image incorporating both functional and anatomical data from the CT and $^{18}$FDG PET images.

### 3.1 Fusion of medical images in a context of multimodality: the wavelet framework

The enhanced image that we are introducing here is computed using a 3D wavelet analysis where details of two images are extracted at different levels of spatial resolution. Considering that the level of resolution of the initial CT image is q, (referred to as CTq) and that of the initial PET image is r = q + p, (referred to as PETr), we can perform the extraction of the spatial frequencies at a level of resolution common to CT and PET (q+p+1), using the "à trous" algorithm. This discrete wavelet transform algorithm was introduced by Dutilleux (Dutilleux, 1987), developed by Holdschneider (Holdschneider et al, 1989) and detailed by Starck (Starck et al, 1998). The process gives an image sequence of coarser and coarser spatial resolution by performing successive convolutions with a low-pass filter h (Boussion et al, 2006).

Practically, at each iteration j, the spatial resolution of the degraded image $\deg_{j-1}$ is degraded to give the degraded image $\deg_j$ according to :

$$\deg_j(k,l) = \sum_{m,n} h(m,n) \deg_{j-1}(k + m2^{j-1}, l + n2^{j-1}) \tag{7}$$

The first approximation image deg0 is taken as I, the original image. The difference $\deg_{j-1} - \deg_j$ is the wavelet coefficients $w_j$ containing the details (edges, texture) at a resolution level between $\deg_{j-1}$ and $\deg_j$. The procedure that reconstructs the original image from its layers of details wk is called synthesis and is given by:

$$\deg_0 = I = I_N + \sum_{k=1}^{k=N} w_k \tag{8}$$

with N the number of iterations from the initial image I to the final degraded image $I_N$ of spatial resolution decreased by $2^N$. The algorithm can be easily implemented by performing the following steps:

1. Initialize j to 0: start with the original image I = deg0 (deg stands for degraded image).
2. Increment j and carry out a convolution of $\deg_{j-1}$ with a low-pass filter h in order to obtain $\deg_j$ (the distance between the central voxel and the adjacent ones is 2j−1).
3. The wavelet coefficients w(j) at this level of resolution are given by $\deg_{j-1} - \deg_j$.
4. If j is less than the required number N of resolutions go to step 2.
5. The set W = $\{w(1), w(2), ..., w(N), \deg_N\}$ is the wavelet transform of I.

In a practical point of vue, zeros are inserted between lines and columns of the filter h at each iteration j of the process. This particularity gives its name to the algorithm "à trous" which in French means "with holes". In the present study, we have chosen a low pass filter corresponding to a B-spline interpolation implemented sequentially according to:

$$h(x,y) = h(x) \otimes h(y) \tag{9}$$

with:

$$h(0) = 3/8, h(\pm 1) = 1/4\ h(\pm 2) = 1/16\ and\ h(n) = 0\ if\ |n| > 2 \tag{10}$$

The initial image can always be perfectly reconstructed by adding the different layers and the final degraded image of the wavelet decomposition on a voxel-to-voxel basis. As a consequence, we have the two following equations:

$$PET_r = PET_{q+p}(x,y,z) = PET_{q+p+1}(x,y,z) + w^{PET}_{q+p+1}(x,y,z) \tag{11}$$

$$CT_q = CT_{q+p+1}(x,y,z) + \sum_{k=1}^{k=p+1} w^{CT}_{q+k}(x,y,z) \tag{12}$$

with $w^{PET}$ and $w^{CT}$ the wavelet coefficients from the wavelet decomposition of respectively (i) the functional PET image of "low" spatial resolution and (ii) the anatomical CT image of "high" spatial resolution. The final enhanced image, or fused image, is then given straightforwardly by:

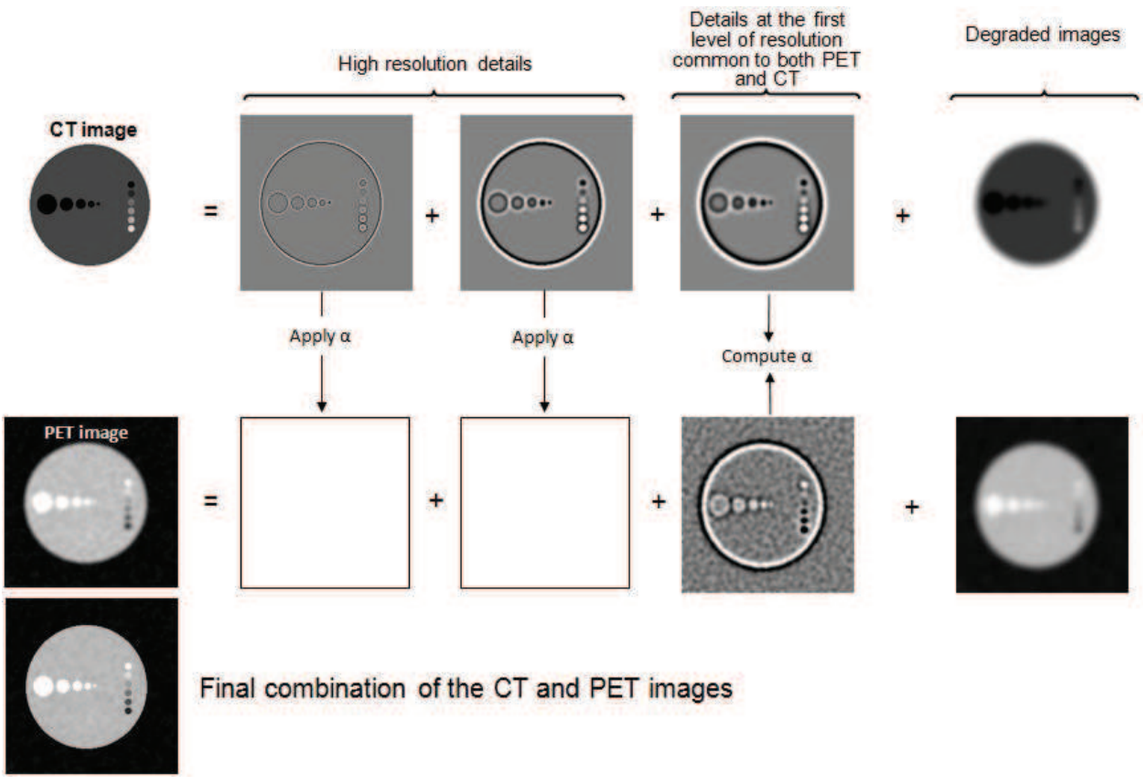


Fig. 5. Illustration of the CT-PET combination process on simulated images. (a) wavelet transform of the original simulated CT image (three iterations were arbitrarily chosen in this example); (b) wavelet transform of the original simulated PET image; the lacking details of the PET image are retrieved from the existing details of the CT images which are modified according to the α model; (c) the fused CT-PET image is the pixel-to-pixel addition of the original PET image with the retrieved details coming from CT.

$$ENH_p(x,y,z) = PET_{q+p+1}(x,y,z) + w^{PET}_{q+p+1}(x,y,z) + \alpha(x,y,z)\sum_{k=1}^{k=p} W^{CT}_{q+k}(x,y,z) \tag{13}$$

where the parameter α is just the mean voxel-to-voxel ratio of wavelet coefficients at resolution q+p+1:

$$\alpha = mean\left(\frac{W^{PET}_{q+p+1}}{W^{CT}_{q+p+1}}\right) \tag{14}$$

In equation (9), each pixel is processed individually and the parameter α is computed locally using a 3D moving cube, simultaneously applied within the PET and CT wavelet layers. For the sake of clarity, the whole process is illustrated on fig. 5 where synthetic images are used in order to facilitate the understanding of the method.

### 3.2 Examples of fused images

Some examples are given on fig. 6 and fig.7 where one can see the transverse view of a CT image, of the corresponding $^{18}$FDG PET image, and of the final fused image.

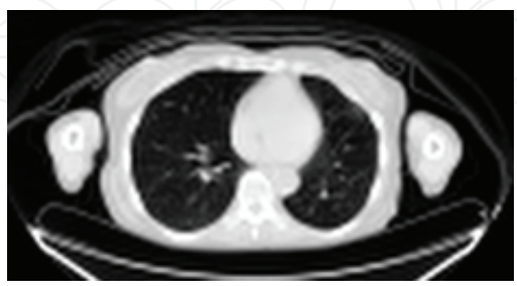

(a)

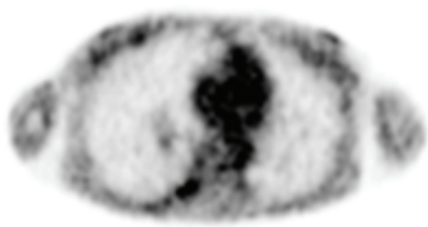

(b)

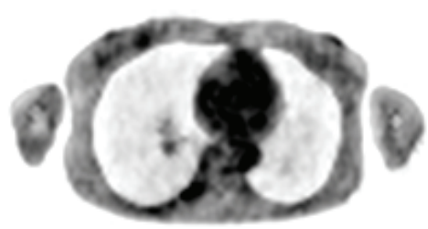

(c)

Fig. 6. Example of CT-PET fusion using wavelet-based decomposition. (a) CT image, (b) PET image and (c) fused CT-PET image, where the contours of the pulmonary lesion become more visible.

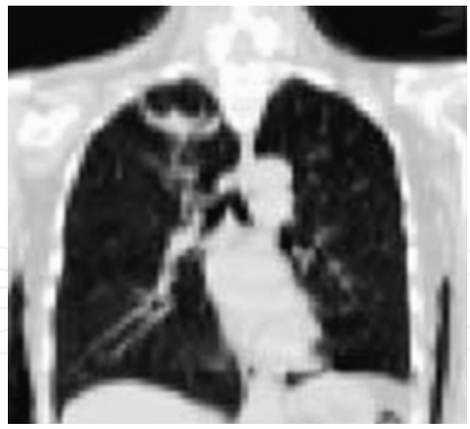

(a)

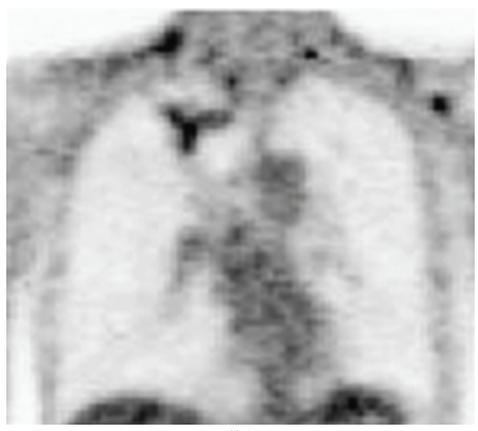

(b)

(c)

Fig. 7. This example is another pertinent illustration of what fusion permits to obtain. In the fused image (c), both anatomical details coming from CT and functional information coming from PET are visible at the same time.

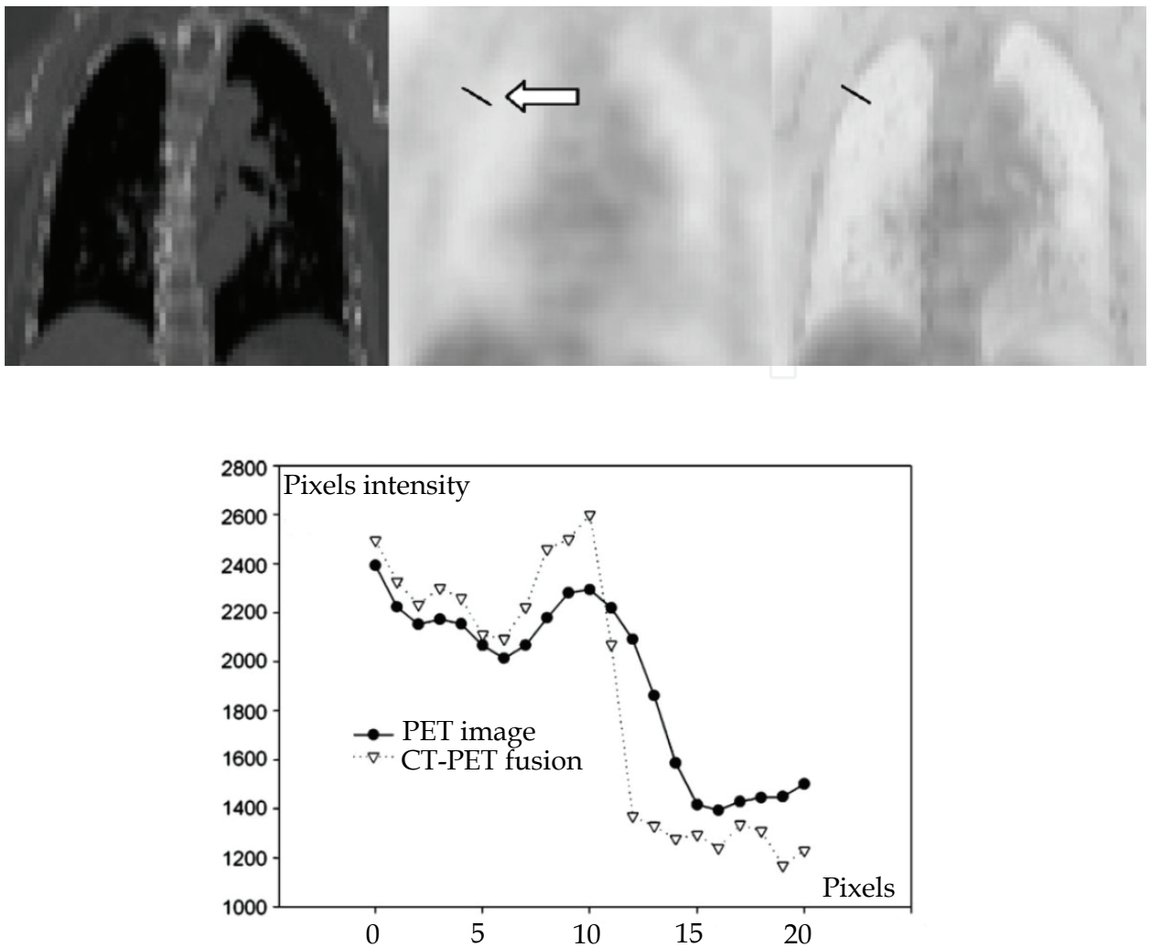


Fig. 8. In this case, we illustrate the fusion with a quantitative analysis of the pixels values along a given profile (see arrow for location). The two curves clearly demonstrate the gain in contrast given by the fusion process. The slope of the curve corresponding to the fused image is sharper than the one corresponding to the original PET image. This improvement if directly coming from the incorporation of high resolution details of the CT image.

### 3.4 Potential improvements

In this part of the study a new approach to CT/PET image fusion has been proposed for whole-body imaging. Contrary to the great majority of existing methods, the aim of the presented work was to provide the user with a fused image preserving both anatomical and functional data. The objective is therefore different from simply presenting two images in a visually convenient fusion display in the sense that quantitative analysis is also here considered as a possible step. In the proposed methodology the anatomical information is present in terms of improved contrast while the intensity in the organs is comparable with the functional information presented by the PET. This is of paramount importance in cancer staging and treatment follow-up for instance, where quantitative assessment of activity

uptake is necessary. Furthermore, for applications in radiotherapy, the efficient image fusion proposed in this article may be of key interest. Indeed, when considering day-to-day clinical use, this algorithm appears user-friendly and allows physicians to gain a lot of time when making diagnosis and when planning radiotherapy treatment on a dedicated software. However, the model that is used to modify the detail layers (images of wavelet coefficient) obtained in the CT decomposition may be considered too simplistic (mean voxel-to-voxel division). A more sophisticated model would be preferable when absolute quantitation is mandatory, for tumour follow-up for example. For this specific purpose we have designed an alternate model which is able to take into account local discrepancies between CT and PET. Adopting a local model may be more appropriate, in particular for limiting artifacts coming from structures present in the CT only. The methodology itself is of course not restricted to whole-body imaging in the oncology domain. Provided two co-registered images are available, one functional and the other anatomical, the process can be applied in a wide range of clinical areas. The main difference with the initial model relies on the definition of the α parameter. In the first method, α is just the global mean of the wavelet ratios (equation 14). In this improved approach (Le Pogam et al, 2008), α is in particular computed locally as a median value instead of a mean value. This point allows improving the quantitative correction of PET images without incorporating artifacts in the final fused image. This original approach is quantitatively relevant in the sense that it leads to a direct correction of partial volume effects.

As an illustration we give an example of partial volume correction in the PET image of a lung lesion (fig.10). In this case, the high resolution details provided by the CT image not only improve the visual aspect of the PET image, but it also corrects the image for the partial volume effect. As a consequence, the direct segmentation of the target for radiotherapy treatment becomes possible.

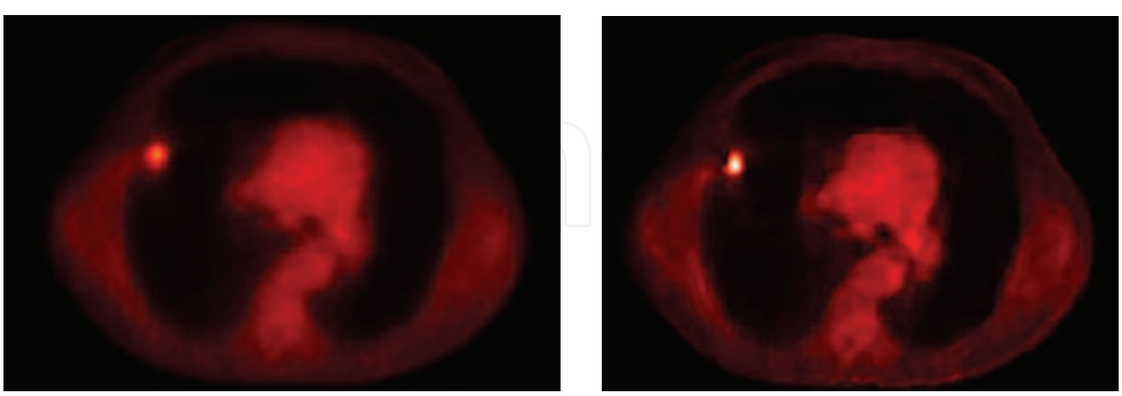

Fig. 10. Original PET image before (left) and after (right) fusion with a corresponding CT image, by using a local model instead of a global one.

## 4. Conclusion

In this chapter we have presented two CT image processing methods dedicated to radiotherapy. X-ray computed tomography is indeed the only image modality mandatory to classical radiotherapy treatment planning. It permits to visualize the anatomy of the patient and in particular to delineate targets and organs at risk. The link between Hounsfield Units and electronic densities also leads to the pre-treatment computation of the dose delivered to the patient. However, new treatment technologies like intensity modulated radiotherapy require more and more data to improve the precision and the efficacy of the treatment delivery. In this context, the monitoring of the respiratory signal and the incorporation of functional imaging in the treatment process are of significant interest. One of the objectives of this chapter was thus to underline the increasing synergy between CT images and others medical signals. The presented studies also illustrated the multi-disciplinary features of modern radiotherapy.

## 5. References

Boussion, N.; Hatt, M.; Lamare, F.; Bizais, Y.; Turzo, A.; Cheze-Le Rest C. & Visvikis, D. (2006). A multiresolution image based approach for correction of partial volume effects in emission tomography. *Phys Med Biol*. Vol 7;51(7), pp 1857-76.

Dutilleux, P. An Implementation of the Algorithme "à trous" to compute the wavelet transform, Proceedings of Congrès ondelettes et méthodes temps-fréquence et espace des phases, Marseille, France, Springer–Verlag, 1987, pp. 298–304.

Gierga D.; Brewer, J.; Sharp, G.; Betke, M.; Willet, C. & Chen, G. (2005) The correlation between external and internal markers for abdominal tumors: implications for respiratory gating. *Int. J. Radiat. Oncol. Biol. Phys*, vol. 61, pp. 1551–1558.

Holdschneider, R.; Kronland-Martinet, R.; Morlet, J. & Tchamitchian, P. (1989). A real time algorithm for signal analysis with the help of the wavelet transform, in: J.M. Combes, et al. (Eds.), Wavelets, Springer–Verlag, Berlin.

Kanoulas, E.; Aslam, J.; Sharp, G.; Berbeco, R.; Nishioka, S.; Shirato H, & Jiang, S. (2007) Derivation of the tumor position from external respiratory surrogates with periodical updating of the internal/external correlation, *Phys. Med. Biol.*, vol. 52, pp. 5443–5456.

Keall, JJ.; Kini, VR.; Vedam, SS. & Mohan R. (2002) Potential radiotherapy improvements with respiratory gating. *Australas. Phys. Eng. Sci. Med.*, vol. 25(1), pp.1–6.

Ledesma-Carbayo, MJ.; Mahia-Casado, P.; Santos, A.; Perez-David, E.; Garcia-Fernandez, MA.; & M Desco. (2006) "Cardiac motion analysis from ultrasound sequences using nonrigid registration: validation against doppler tissue velocity," *Ultrasound Med. Biol.*, vol. 32, pp. 483–490.

Le Pogam, A.; Boussion, N.; Hatt, M.; Turkheimer, F.E.; Prunier-Aesch, C.; Guilloteau, D.; Baulieu, J.L. & Visvikis, D. (2008). A 3D multi resolution local analysis approach for correction of partial volume effects in emission tomography. *Proceedings of Nuclear Science Symposium Conference Record*.pp 5300-5303.

McClelland, JR.; Blackall, JM.; Tarte, S.; Chandler, AC.; Hughes, S.; Ahmad, S. Landau, DB.; Hawkes, DJ. (2006) A continuous 4d motion model from multiple respiratory cycles for use in lung radiotherapy. *Med. Phys.*, vol. 33, pp. 3348–3358.

McClelland, JR.; Gao, G.; Tarte, S.; Blackall, JM.; Hughes, S.; Chandler, AC.; Ahmad, S. Landau, DB.; Hawkes, DJ. (2008) Removing artifacts from 4dct volumes acquired in cine mode using b-spline non-rigid registrations. 50th Annual Meeting AAPM, Med. Phys, vol. 35, p. 2992.

Pan, T.; Sun, X.; & Luo, D. (2007). Improvement of the cinect based 4d-ct imaging. *Med. Phys.*, vol. 34(11), pp. 4499–4503.

Rietzel E, Chen GTY, Choi NC, & Willet CG. (2005) Four-dimensional image-based treatment planning: target volume segmentation and dose calculation in the presence of respiratory motion. *Int J Radiat Oncol*, vol. 61, pp. 1535–1550.

Seungyong, L.; Wolberg, G. & Shin, SY. (1997). Scattered data interpolation with multilevel b-splines, *IEEE Trans. Vis. Comput. Graph.*, vol. 3(3), pp. 228–244.

Starck, JL.;, Murtagh, F.; Bijaoui, A. (1998). *Image processing and data analysis: the multiscale approach*, Cambridge University Press, Cambridge, UK.

Vedam, SS.; Keall PJ.; Kini VR. & Mohan R. (2001). Determining parameters for respiration-gated radiotherapy. *Med. Phys.*, vol. 28, pp. 2139–2146.

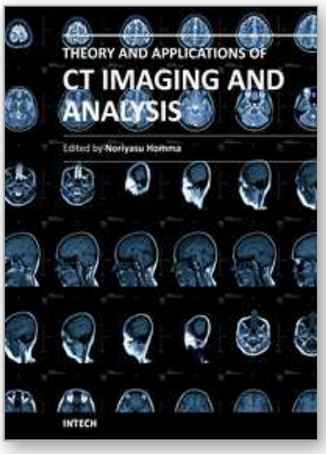


**Theory and Applications of CT Imaging and Analysis**

Edited by Prof. Noriyasu Homma

ISBN 978-953-307-234-0

Hard cover, 290 pages

**Publisher** InTech

**Published online** 04, April, 2011

**Published in print edition** April, 2011

The x-ray computed tomography (CT) is well known as a useful imaging method and thus CT images have continuingly been used for many applications, especially in medical fields. This book discloses recent advances and new ideas in theories and applications for CT imaging and its analysis. The 16 chapters selected in this book cover not only the major topics of CT imaging and analysis in medical fields, but also some advanced applications for forensic and industrial purposes. These chapters propose state-of-the-art approaches and cutting-edge research results.

**How to reference**

In order to correctly reference this scholarly work, feel free to copy and paste the following:

Boussion Nicolas, Fayad Hadi, Le Pogam Adrien, Pradier Oliver and Visvikis Dimitris (2011). Image Processing Methods in CT for Radiotherapy Applications, Theory and Applications of CT Imaging and Analysis, Prof. Noriyasu Homma (Ed.), ISBN: 978-953-307-234-0, InTech, Available from: http://www.intechopen.com/books/theory-and-applications-of-ct-imaging-and-analysis/image-processing-methods-in-ct-for-radiotherapy-applications

INTECH
open science | open minds

**InTech Europe**
University Campus STeP Ri
Slavka Krautzeka 83/A
51000 Rijeka, Croatia
Phone: +385 (51) 770 447
Fax: +385 (51) 686 166
www.intechopen.com

**InTech China**
Unit 405, Office Block, Hotel Equatorial Shanghai
No.65, Yan An Road (West), Shanghai, 200040, China
中国上海市延安西路65号上海国际贵都大饭店办公楼405单元
Phone: +86-21-62489820
Fax: +86-21-62489821

© 2011 The Author(s). Licensee IntechOpen. This chapter is distributed under the terms of the Creative Commons Attribution-NonCommercial-ShareAlike-3.0 License, which permits use, distribution and reproduction for non-commercial purposes, provided the original is properly cited and derivative works building on this content are distributed under the same license.